Measurement report: Characterization and source apportionment of coarse particulate matter in Hong Kong: Insights into the constituents of unidentified mass and source origins in a coastal city in southern China

5 Yee Ka Wong[1,*], Kin Man Liu[2], Claisen Yeung[2], Kenneth K. M. Leung[3], Jian Zhen Yu[1,4,*]

[1]Division of Environment and Sustainability, Hong Kong University of Science and Technology, Clear Water Bay, Kowloon, Hong Kong
[2]Environmental Central Facility, Hong Kong University of Science and Technology, Clear Water Bay, Kowloon, Hong Kong
[3]Hong Kong Environmental Protection Department, 15/F, East Wing, Central Government Offices, 2 Tim Mei Avenue, Tamar,
10 Hong Kong
[4]Department of Chemistry, Hong Kong University of Science and Technology, Clear Water Bay, Kowloon, Hong Kong

Correspondence to: Yee Ka Wong (envrykwong@ust.hk); Jian Zhen Yu (jian.yu@ust.hk)

Abstract. Coarse particulate matter (i.e., PM with aerodynamic diameter between 2.5 and 10 micrometers or PM_{coarse}) has been increasingly recognized of its importance in PM_{10} regulation because of its growing proportion in PM_{10} and the
15 accumulative evidence for its adverse health impact. In this work, we present comprehensive PM_{coarse} speciation results obtained through a one-year long (January 2020–February 2021) joint PM_{10} and $PM_{2.5}$ chemical speciation study in Hong Kong, a coastal and highly urbanized city in southern China. The annual average concentration of PM_{coarse} is 14.9 ± 8.6 μg m^{-3} ($\pm$standard deviation), accounting for 45 % of PM_{10} (32.9 ± 18.5 μg m^{-3}). The measured chemical components explain ~75 % of the PM_{coarse} mass. The unexplained part is contributed by unmeasured geological components and residue liquid water
20 content, supported by analyses by positive matrix factorization (PMF) and the thermodynamic equilibrium model ISORROPIA II. The PM_{coarse} mass is apportioned to four sources resolved by PMF, namely soil dust/industrial and coal combustion, construction dust/copper-rich emissions, fresh sea salt, and an aged sea salt factor containing secondary inorganic aerosols (mostly nitrate). The PM_{coarse} concentration and source composition exhibit a distinct seasonal variation, a result mainly driven by the source areas the air masses have travelled as revealed by back-trajectory analysis. In summer when the site is dominated
25 by marine air mass, PM_{coarse} is the lowest (average = 8.1 μg m^{-3}), and sea salt is the largest contributor (47 %), followed by the two dust factors (36 % in total). In winter when the site receives air mass mainly from the northern continental region, PM_{coarse} concentration triples (24.8 μg m^{-3}), with the two dust factors contributing three quarters of the aerosol mass. The potential dust source areas are mapped using the Concentration-Weighted Trajectory technique, showing either the Greater Bay Area or the greater part of southern China as the origin of fugitive dust emissions leading to elevated ambient PM_{coarse} loadings in Hong
30 Kong. This study, first of this kind in our region, provides highly relevant guidance to other locations with similar monitoring

needs. Additionally, the study findings point to the needs for further research on the sources, transport, aerosol processes, and health effects of PM_{coarse}.

1 Introduction

Coarse particulate matter (PM_{coarse}), defined as PM with aerodynamic diameter of 2.5–10 μm in the World Health Organization's air quality guidelines, play important roles in air quality, public health, and global climate. Progress in reducing fine PM ($PM_{2.5}$) pollution in the past makes it increasingly important to explore possibilities to control PM_{coarse} for PM_{10} regulation. In the United States, PM_{coarse} constitutes half of PM_{10} mass nationwide in 2012–2016 (Hand et al., 2019). The relative contribution of PM_{coarse} to PM_{10} mass was reported to increase by 0.7–1.2 % annually over 2000–2016. While the health impact of PM_{coarse} examined by earlier epidemiological studies were inconclusive (Adar et al., 2014), more recent epidemiological studies in China showed evidence for the adverse health impact of PM_{coarse} (Chen et al., 2019; Lei et al., 2022). The health impact of PM_{coarse} depends on the exposure to and concentration and composition of PM_{coarse}, which may explain the varied health implications found in different studies (Adar et al., 2014; Chen et al., 2019; Lei et al., 2022).

Understanding the sources of PM_{coarse} is important for developing control strategies. PM_{coarse} is primarily generated by mechanical processes such as wind and erosion, and the sources can be naturally and anthropogenically related. The natural processes include ejection of sea spray, resuspension of soil dust, and release of plant-related particles, etc. Common anthropogenic PM_{coarse} sources include road dust resuspended by road traffic, brake/tire wearing, construction dust, fly ash and metallurgical process. While PM_{coarse} are mostly directly emitted, certain components in PM_{coarse} can be related to secondary formation. For example, nitrate in the coarse mode is formed by the reaction between nitric acid (HNO_3) from oxidation of NO_x and preexisting alkaline aerosols, such as sea salt and dust particles (Bian et al., 2014). A recent study showed that mineral dust can serve as a medium for rapid secondary inorganic and organic aerosol formation under high photochemical activity and relative humidity conditions, which has important implications to the life cycle of secondary aerosols (Xu et al., 2020). PM_{coarse} also exerts an impact on earth's climate because of its continuous loading in the atmosphere and its ability to scatter and absorb radiation or act as cloud condensation and ice nuclei (USEPA, 2019).

As a coastal and highly urbanized city and being a part of the Guangdong–Hong Kong–Macao Greater Bay Area (GBA) economic and business hub in southern China, Hong Kong is facing atmospheric PM pollution originated from both local and regional influence. Continuous improvement in local and regional PM concentrations is noted in the last few years (HKEPD, 2020). The ambient PM_{10} concentration has been reduced by 24 % from 42 μg m^{-3} in 2012 to 32 μg m^{-3} in 2019. The reduction was contributed mostly by $PM_{2.5}$, which correspondingly decreased by 32 % from 28 to 19 μg m^{-3}. By taking the difference between PM_{10} and $PM_{2.5}$, it can be deduced that PM_{coarse} only decreased slightly from 14 to 13 μg m^{-3} in the corresponding period. Because of the disproportionate reduction in $PM_{2.5}$, the relative contribution of PM_{coarse} to PM_{10} increased from 33 % in 2012 to 41 % in 2019. The analysis has two important implications. First, $PM_{2.5}$ and PM_{coarse} in Hong Kong have different

sources. Second, it is important to characterize the sources of PM_{coarse}, which has gained increasing importance in PM_{10} contribution.

Previous PM_{coarse} studies in Hong Kong were focused on suburban coastal area (Cohen et al., 2004), roadside environment (Cheng et al., 2015), and public transport micro-environments (Jiang et al., 2017). These studies provide limited representation of the general PM_{coarse} pollution characteristics given the predisposition to the influence by nearby sources; for example, sea spray in coastal environment or traffic-related emissions in roadside environment. Hong Kong has been operating a PM_{10} monitoring network since 1998, which consists of six general stations and one roadside station. The network collects 24 h samples on quartz fiber filters on a 1 in 6 days schedule by high-volume (HV) samplers, which operate at a flow rate of 1.13 $m^3\ min^{-1}$. The HV quartz fiber filters are used for gravimetric analysis and chemical speciation including major ions, elements, organic carbon (OC), and elemental carbon (EC) (Zhang et al., 2018). The $PM_{2.5}$ speciation network in Hong Kong started to operate in 2011. $PM_{2.5}$ samples are collected on Teflon filters and quartz fiber filters by middle-volume samplers which operate at a flow rate of 16.7 L min^{-1}. The Teflon filters are used for gravimetric and elemental analyses while the quartz fiber filters are analyzed for major ions, OC and EC (Yu and Zhang, 2018). It should be noted that Si and Ti, which are important markers for quantifying dust contribution, are not determined in PM_{10} samples due to the high background in ICP-OES analysis. On the other hand, the $PM_{2.5}$ network employs X-ray fluorescence technique for elemental analysis, and thus has no difficulty in reporting the concentrations of these two elements. Additionally, carbonaceous components in PM_{10} and $PM_{2.5}$ are determined using different thermal methods (NIOSH protocol for PM_{10} and IMPROVE protocol for $PM_{2.5}$). In view of the aforementioned, the two PM monitoring networks in Hong Kong adopt different sampling and laboratory analysis protocols which would introduce uncertainties to the analysis results. The possibility of deriving a solid understanding of the composition and sources of PM_{coarse} using existing data sets certainly requires further investigation.

We present in this work the first joint PM_{10} and $PM_{2.5}$ speciation effort in Hong Kong in which all the sampling and chemical analysis work were conducted using identical methods and by the same laboratory. The aim is to obtain high quality composition data for PM_{coarse}. It has been reported in a number of studies that a notable fraction of PM_{coarse} was often unable to be identified. Cheung et al. (2011) reported an up to 25 % contribution from such unidentified mass in Los Angeles area, while Putaud et al. (2010) reported 6–43 % in urban Europe. Although it has been suggested that the unidentified mass was associated with liquid water content and mineral components, their exact contributions have remained largely uncharacterized. By using positive matrix factorization (PMF), we showed that the unidentified masses can be allocated to the resolved sources, providing qualitative and quantitative information on their origins. We propose the unidentified mass in PM_{coarse} in our study region is mainly composed of unmeasured mineral components and liquid water content. The measured PM_{coarse} in its entirety was successfully apportioned to various contributing sources by PMF, and the potential source origins are identified using backward air mass trajectory analysis. With the robust source apportionment analysis, we found that fugitive dust associated with regional influence is the dominant contributor of high PM_{coarse} loading in Hong Kong. The methodology and results from this study can serve to provide guidance to other locations with similar monitoring needs.

2 Methods

2.1 Ambient sampling

Aerosol sampling was conducted in Hong Kong at the Tuen Mun Air Quality Monitoring Station (TMC AQMS), which is located on the rooftop of a public library building (22°23'28.4" N, 113°58'37.1" E, ~30 m above ground level). The AQMS is situated in the northwestern part of the Hong Kong. The city, with a territory area of ~1110 km^2 and a population of ~7.5 million, is part of the larger economic and business hub, the Greater Bay Area (GBA) (~56,000 km^2, population of ~85 million), in Guangdong province of China. Located in the sub-tropical region along the southeast coast of China, Hong Kong exhibits a season-dependent air pollution characteristics that is closely related to the seasonal evolution of the East Asian Monsoon system. Generally, air pollution during colder seasons is more severe than in warm seasons. This will be elaborated when the measurement results are discussed.

Twenty-four-hour samples (midnight to midnight) for PM_{10} and $PM_{2.5}$ were collected simultaneously on a once every three days schedule. The sampling lasted for over a year from 18 January 2020 to 9 February 2021. In each sampling event, one 47-mm Teflon and one 47-mm quartz fiber filter samples were collected for each of the PM size fractions. The sample collection was accomplished by deploying two pairs of federal reference method samplers operated at a flow rate of 16.7 L min^{-1}. The first pair (Partisol Plus 2025, Thermo Fisher Scientific, MA, USA) were equipped with PM_{10} sampling inlets to collect PM_{10}, whereas in the second pair (BGI PQ200, Mesa Labs, CO, USA) the Very Sharp Cut Cyclones were installed downstream of the PM_{10} inlets for $PM_{2.5}$ fine particles collection. Field blanks (Teflon and quartz) were collected during the last sampling of each month. All the filter samples were delivered back to the balance laboratory for conditioning followed by gravimetric analysis within one week. The filters were subsequently stored at –20ºC until chemical analysis.

2.2 Mass and chemical composition determination for PM_{coarse}

The mass concentration and chemical composition of PM_{coarse} are determined as the difference between PM_{10} and $PM_{2.5}$ measurements. The PM_{10} and $PM_{2.5}$ samples were speciated using the identical protocol that has been adopted in the Hong Kong $PM_{2.5}$ speciation network for regular monitoring of $PM_{2.5}$ composition since 2011 (Huang et al., 2014). The protocol is based on the speciation guideline by the U.S. Environmental Protection Agency (Chow and Watson, 1998). The design of joint sampling and chemical analysis of PM_{10} and $PM_{2.5}$ eliminates data incompatible issues observed for data from the existing networks.

All the gravimetric and chemical analyses of the filter samples were conducted by the same laboratory in the Hong Kong University of Science and Technology. PM mass concentration was determined on the Teflon filter samples by gravimetry with a digital microbalance (Sartorius AG, Model MC 5-0CE, Göttingen, Germany, sensitivity of ±1 μg) under a temperature- and relative humidity-controlled environment (20–23 °C and 30–40 %). Elements from Al to U were quantified on the Teflon filters by an energy dispersive X-ray fluorescence spectrometer (ED-XRF) (Epsilon 5, PANalytical, The Netherlands). OC and

EC were quantified on the quartz fiber filters with an aerosol carbon analyzer (DRI Model 2001A, Atmoslytic, Calabasas, CA, USA) based on the thermal/optical reflectance method, adopting the IMPROVE_A temperature protocol (Chow et al., 2007). Ionic species including Cl^-, NO_3^-, SO_4^{2-}, NH_4^+, Na^+, Mg^{2+}, K^+ and Ca^{2+} were analyzed on the quartz fiber filters by ion chromatography (IC) (Dionex ICS-1100, Thermo Fisher Scientific, MA, USA).

130   The species concentrations in PM_{10} and $PM_{2.5}$ samples were blank corrected. The measurement precisions were propagated from the precisions of volumetric measurements during sampling, chemical analyses, and field blank variability (Yu and Zhang, 2018). Duplicate analysis of the aerosol samples was performed for every 10 measurements to derive precisions for the chemical analyses. The measurement precisions for PM_{coarse} speciation were propagated from the precisions of the PM_{10} and $PM_{2.5}$ measurements.

135   **2.3 Source apportionment by positive matrix factorization**

Source identification and quantification for PM_{coarse} was conducted by analyzing the speciation data matrix with positive matrix factorization (PMF). PMF decomposes the speciation data matrix into factor profiles and factor contributions matrices with non-negative constraints, with the objective of minimizing the uncertainty weighted differences between observed and apportioned species concentrations represented by an objective function Q (Paatero and Tapper, 1994). The USEPA PMF 5.0

140   software was used for this undertaking (Norris et al., 2014). The fitting species include total PM_{coarse} mass and a suite of chemical species including Na^+, NH_4^+, Mg^{2+}, Cl^-, NO_3^-, SO_4^{2-}, OC, EC, Al, Si, K, Ca, Ti, V, Mn, Fe, Ni, Cu, Zn, and Pb. The measurement precisions for each species in each sample described in Sect. 2.2 were used as the uncertainty inputs for the PMF modeling. The uncertainty of PM_{coarse} mass was tripled to downweigh its influence in the source apportioning. This allows the total PM_{coarse} mass to be apportioned mainly according to its covariance with other species. Concentrations below the method

145   detection limit (MDL) were replaced by $1/2 \times$ MDL with corresponding uncertainties set to be $5/6 \times$ MDL as recommended in the PMF user manual. The input speciation data matrix consists of 123 PM_{coarse} samples.

3 Results and discussion

3.1 Abundance and composition of PM_{coarse}

3.1.1 Annual average and comparison with other locations

150   The speciation data quality was evaluated by examining the consistency between species concentrations measured by different methods; for example, gravimetric mass vs. mass from continuous monitor, gravimetric mass vs. reconstructed mass, SO_4^{2-} vs. total S, and K^+ vs. total K, etc. Deming regression was applied in the examination using the Scatter Plot computer program developed by Wu, which is available at https://doi.org/10.5281/zenodo.832417 (Wu and Yu, 2018). This technique is applied to consider the measurement uncertainties of both variables to be compared in the regression. Details of the evaluation are

155 provided in Sect. S1 in the Supplement. In short, the evaluation shows the speciation data are of adequate quality for the ensuing analyses.

The study-wide average concentration of PM_{coarse} is 14.9 ± 8.6 µg m^{-3} (±standard deviation), accounting for 45 % of ambient PM_{10} (32.9 ± 18.5 µg m^{-3}). The daily concentrations range from 2.9 to 40.4 µg m^{-3}. The contribution of geological material is estimated by assuming the crustal elements are in oxide forms, i.e., $1.89\times[Al] + 2.14\times[Si] + 1.2\times[K] + 1.4\times[Ca] + 1.67\times[Ti]$

160 $+ 1.43\times[Fe]$. This component has the largest contribution, making up 5.2 µg m^{-3} or 35 % of the PM_{coarse} mass. The next important component is nitrate (2.2 µg m^{-3}, 15 %), followed by sea salt-related ions (i.e., Na^+, Mg^{2+}, and Cl^-) and organics, which represent 11 % and 8 %, respectively. The coarse organics were estimated by multiplying the measured OC with a factor of 2, assuming the organics are mainly associated with biological particles, which are enriched in oxygenated compounds such as polyols and carboxylic acids (Edgerton et al., 2009). The composition forms a stark contrast with that of $PM_{2.5}$ (18.0 ± 11.2

165 µg m^{-3}), in which carbonaceous components (organics and EC, 41 %) and secondary ions (NH_4^+, NO_3^-, and SO_4^{2-}, 38 %) are the major components. The difference is consistent with combustion and secondary aerosol formation processes being the major sources of fine particles, whereas coarse particles are primarily generated by mechanical processes. The organics here were approximated to be $1.6\times[OC]$ considering typical features of urban aerosols with both primary and secondary contributions (Turpin and Lim, 2001).

170 The annual average concentrations of PM_{coarse} and selected major components measured in this study are compared with those in other locations in Table 1. Only studies that spanned at least one year or more and had all major species measured (i.e., elements, ions, OC and EC) are considered. Our PM_{coarse} level is amid those in other urban locations, more than 2 times higher than Milan in Italy and ~5 µg m^{-3} higher than Central Los Angeles, and only half of that in Casa Grande in Arizona and a tenth of Lahore in Pakistan. Our concentration is also comparable to two roadside studies carried out in Bern in Switzerland and in

175 London and Birmingham in the UK. We note the PM_{coarse} concentration in a Hong Kong roadside study is ~10 µg m^{-3} higher than the current study. Yet a straightforward urban vs. roadside comparison is not feasible given the roadside measurement was conducted more than 15 years ago. We also note that all the cited measurements were taken at least a decade ago. The lack of more recent measurements highlights the need for more PM_{coarse} speciation effort, considering the growing importance of PM_{coarse} in aerosol mass loading and health effect contributions as $PM_{2.5}$ has been controlled effectively in many locations.

180 Our PM_{coarse} concentration is also 3–4 times lower than that measured in desert area in Arizona but one-third higher than a desert-like area in Lancaster in Los Angeles.

Geological material is the single largest component in PM_{coarse} across all studies including ours, accounting for roughly 30–50 % (Lahore shows 74 %), underlining the importance in identifying fugitive dust sources (e.g., natural vs. anthropogenic) for effective mitigation of PM_{coarse}. We note that our nitrate concentration is the highest among all studies (except for the Lahore

185 study, which is comparable to ours), constituting 2.2 µg m^{-3} or 15 % of the PM_{coarse}. Coarse mode nitrate mainly forms by the uptake of HNO_3 by pre-existing alkaline particles forming $NaNO_3$ in reaction with sea salt and $Ca(NO_3)_2$ with soil dust (Bian et al., 2014). Our total carbon level of 0.7 µg C m^{-3} is among the lowest compared to other studies, with 86 % of it coming

from OC. A quarter of PM$_{coarse}$ mass is regarded as unidentified in this study. The percentage share is among those observed in other studies, which range between 8 % and 38 %. The nature of the unidentified mass will be discussed in Sect. 3.2.2.

3.1.2 Seasonal variations in PM$_{coarse}$ mass and composition

The seasonal evolution of weather in Hong Kong is largely driven by the East Asian Monsoon system. Correspondingly, the atmospheric PM pollution in Hong Kong displays a distinct seasonal characteristic. In general, the PM loading in summer is mainly governed by local emissions due to the prevailing southerlies carrying clean marine air mass. In winter, the prevailing northerlies place Hong Kong under the immediate downwind of the continental region with intense industrial and agricultural activities. Under this situation, the PM loading is affected by both local and regional sources. The transient seasons – spring and fall – have more mixed wind directions. The seasonal contrast in precipitation frequency and ambient temperature, both being higher in summer and lower in winter, also contributes to the variation in PM concentration across different seasons (Louie et al., 2005; Yu et al., 2004).

The sampling period in this study is divided into four seasons based on the observed meteorological and weather patterns as analyzed in Sect. S2 in the Supplement. Table 2 lists the starting and ending dates of individual seasons, along with the seasonal averages of PM concentrations and several meteorological parameters. Note that the two winter periods at the beginning and the end of the sampling program are regarded as two different winter periods considering the variability in weather conditions and that they span mostly different calendar months.

Figure 1 presents the PM$_{coarse}$ concentration and composition by season. The PM$_{coarse}$ exhibits a significant variation across different seasons, ranging from the lowest 8.1 μg m^{-3} in summer to the highest 24.8 μg m^{-3} in second winter. Washout by precipitation plausibly play a role in the seasonal contrast, given that summer takes up 75 % of the rainfall for the whole study period (Table 2). Mixing layer height appears to play an insignificant role in controlling the variation in PM$_{coarse}$ level. For example, although the mixing height in the first winter is the lowest among all seasons (509±402 m) while that in the second winter is the highest (874±408 m), the PM$_{coarse}$ in the latter is more than twice higher than the former. The wind speed also shows small variation across the seasons, with a range of 1.9 to 2.3 m s^{-1}. This range corresponds to a Beaufort Scale Number of 1–2, referring to the light wind condition. The meteorological data imply changes in emission pattern and/or air mass origin are likely responsible for the seasonal variation in PM$_{coarse}$ levels.

The composition information indicates that geological material is largely responsible for the variability in PM$_{coarse}$. This component takes up 22–43 % of the PM$_{coarse}$ mass. The seasonal contrast in the contribution of this component could be attributed to enhanced wet deposition in warmer season and elevated contribution from regional transport in colder season. The unidentified mass also represents a major component in most seasons (except spring), accounting for 20–32 % of PM$_{coarse}$ mass. Like geological material, this fraction has a significantly enhanced contribution in the colder season compared to the warmer season. As for other components, nitrate has the highest absolute contribution in spring and lowest in summer (3.2 vs. 1.2 μg m^{-3}). Organics are the highest in the second winter and lowest in the first winter, showing an order of magnitude

difference (2.5 vs. 0.2 µg m^{-3}). The concentrations of sea salt-related ions (i.e., Na$^+$, Mg^{2+}, and Cl$^-$) are higher in the warmer season than that in colder season, which is consistent with the enhanced influence of marine air mass in the warmer season.
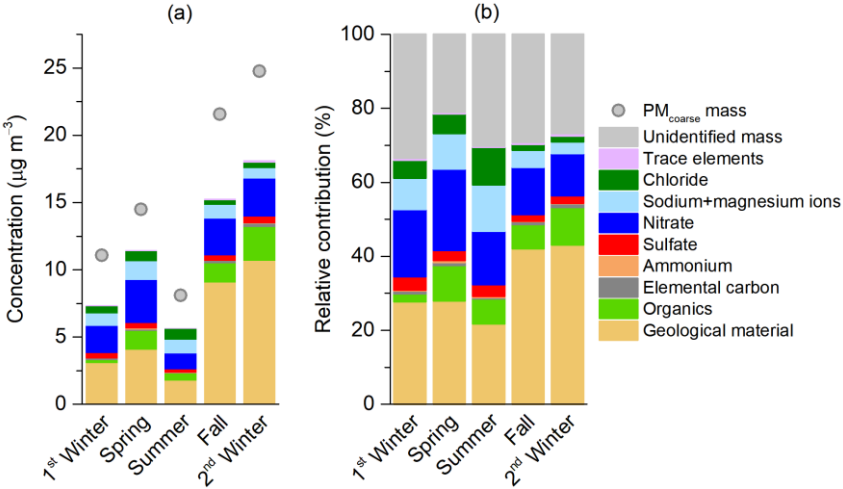
Figure 1. Seasonal variations in concentration and composition of PM$_{coarse}$ observed at the Tuen Mun Air Quality Monitoring Station in Hong Kong. Figure (a) and (b) show the results in absolute concentration and relative contribution, respectively.

Table 1. Comparison of PM$_{coarse}$ concentration and major composition in microgram per cubic meter (percentage contribution to PM$_{coarse}$ shown in parentheses) in Hong Kong and measurements in other locations

Location	Measurement period	Number of measurements	PM$_{coarse}$	Geological material	Nitrate	Total carbon	Unidentified mass	Investigator
Urban								
Hong Kong	Jan. 2020–Feb. 2021	123	14.9	5.2 (35)[a]	2.2 (15)	0.7 (5)	4.1 (26)	This study
Milan, Italy	Dec. 2009–Nov. 2010	~50	6.8	2.2 (32)[b]	<0.9 (13)[d]	0.7 (10)	2.6 (38)	Daher et al., 2012
Central Los Angeles	Apr. 2008–Mar. 2009	~50	10.1	2.3 (23)[b]	1.9 (19)	1.1 (11)	1.9 (18)	Cheung et al., 2011
Casa Grande, Arizona	Feb. 2009–Feb. 2010	~60	30.6	16.4 (54)[b]	0.7 (2)	1.9 (6)	7.4 (24)	Clements et al., 2014
Lahore, Pakistan	Jan. 2007–Jan. 2008	63	142	105 (74)[b]	2.4 (2)	7.5 (5)	24.1 (17)	Stone et al., 2010
Roadside								
London and Birmingham	Apr. 2000–Jan. 2002	101	12.4	4.7 (38)[c]	1.4 (11)	2.1 (17)	0.9 (8)	Harrison et al., 2004
Bern, Switzerland	Apr. 1998–Mar. 1999	76	19.6	4.9 (25)[b]	1.1 (6)	3.7 (19)	4.4 (23)	Hueglin et al., 2005
Hong Kong	Oct. 2004–Sep. 2005	40	25.9	7.3 (28)[a]	1.9 (7)	3.8 (15)	6.7 (26)	Cheng et al., 2015
Desert								
Lancaster, Los Angeles	Apr. 2008–Mar. 2009	~50	9.4	3.6 (38)[b]	0.5 (5)	0.6 (6)	3.4 (36)	Cheung et al., 2011
Pinal County, Arizona	Feb. 2009–Feb. 2010	~60	45.5	23.5 (52)[b]	0.8 (2)	2.1 (5)	13.6 (30)	Clements et al., 2014

Cowtown, Arizona	Feb. 2009–Feb. 2010	~60	66.6	31.1 (47)[b]	0.8 (1)	8.6 (13)	11.3 (17)	Clements et al., 2014

[a] Estimated by the investigators assuming oxides form of crustal elements.

[b] Estimated by the investigators assuming [Si] = 3.4×[Al] since Si was not measured.

[c] Estimated by the investigators using Ca and Fe as the markers for gypsum and soil dust, respectively.

230 [d] Only aggregate ions concentration was reported by the investigators.

Table 2. Summary of season division, PM concentrations, and meteorological parameters in Tuen Mun during the sampling period

Season	Period	Number of aerosol samples	PM_{coarse} ($\mu g\ m^{-3}$)	$PM_{2.5}$ ($\mu g\ m^{-3}$)	Temperature (ºC)	Relative humidity (%)	Wind speed ($m\ s^{-1}$)	Total precipitation (mm)	Mixing height (m)
First winter	18 Jan.–9 Mar. 2020	16	11.1	16.7	18.7±3.7	76±14	1.9±1.3	29.2	509±402
Spring	10 Mar.–17 May 2020	23	14.5	19.2	23.1±3.6	81±13	2.1±1.3	72.1	742±467
Summer	18 May–7 Oct. 2020	42	8.1	9.5	28.1±2.0	82±10	2.3±1.3	315.7	837±363
Fall	8 Oct.–28 Nov. 2020	18	21.6	22.3	23.5±2.5	67±14	2.2±1.2	1.5	870±425
Second winter	29 Nov. 2020–9 Feb. 2021	24	24.8	29.5	16.4±3.8	60±17	2.3±1.6	0.0	874±408

3.2 Source characterization for PM_{coarse}

3.2.1 Source identification by PMF analysis

235 Here the source origins of PM_{coarse} are discussed. The number of factors (or source categories) contributing to PM_{coarse} was determined in the PMF analysis. The PMF solution with four factors was selected for source interpretation after an examination of the physical interpretability of the resolved factor profiles for a series of PMF solutions with different factor numbers. The details are provided in Sect. S3 in the Supplement. In brief, the 3-factor solution was discarded as it gave poor modeling result for Cu, which is an important species in PM health effects associated with reactive oxygen species formation (Bates et al.,

240 2019). The 5-factor solution was not considered either, because the fifth factor, which is a secondary nitrate factor, was assessed to be chemically inexplainable after examining the charge balance of the ionic composition. The stability of the 4-factor solution has been tested against the bootstrapping and displacement functions embedded in the PMF software. The results show that the PMF solution is statistically robust for source analysis. Details of the uncertainty estimation are summarized in Table S2 in the Supplement.

245 The factor profiles resolved in the 4-factor solution are shown in Fig. 2. The four factors can be broadly classified into the sea salt category consisting of the first and second factors, and the dust category consisting of the third and fourth factors. The first factor is marked by the high loading of Cl^- with additional presence of Na^+ and Mg^{2+}, which are strong indicators for fresh sea salt. The molar equivalent of Cl^- is balanced by that of Na^+ and Mg^{2+}, and it has an anion-to-cation equivalence ratio of 0.99, adding credence to the validity of this factor. The second factor is loaded with a substantial fraction of Na^+ and Mg^{2+}, which

250 are markers for sea salt. The absence of Cl^- and presence of NO_3^- indicate this factor specifically represents aged sea salt,

given that Cl⁻ in sea salt is actively depleted by gaseous HNO₃ forming nonvolatile NaNO₃ (Bian et al., 2014). This factor is termed aged sea salt mixed with secondary inorganic aerosols. The third and fourth factors are clearly associated with fugitive dust, as indicated by the high abundance of crustal elements (e.g., Al, Si, Ca, Ti, and Fe). However, the chemical fingerprints in these two factor profiles only provide limited information for pinpointing the more specific sources responsible for the aerosol burden.
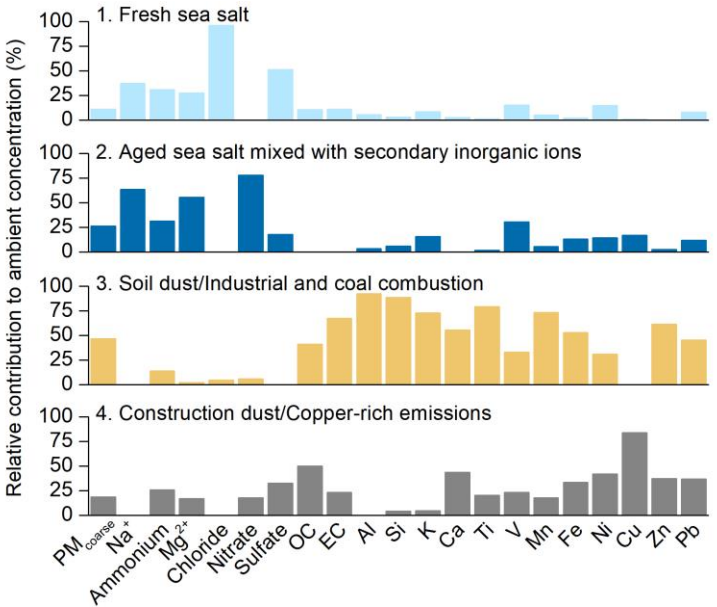
Figure 2. Factor profiles resolved by positive matrix factorization for source apportionment of PM$_{coarse}$ measured at Tuen Mun Air Quality Monitoring Station in Hong Kong.

3.2.2 Source identification by backward air mass trajectory analysis

To better understand the sources behind the PMF-resolved factors, the association between air mass origins and source contributions was investigated through backward air mass trajectory analysis. The back-trajectories were computed by the Hybrid Single-Particle Lagrangian Integrated Trajectory (HYSPLIT) model using meteorological data from the 1° horizontal resolution Global Data Assimilation System (Stein et al., 2015). Past 48-hour back-trajectories of air mass reaching Hong Kong at 300 m height at the end of each sampling event at midnight were computed. The trajectories were clustered based on similarity between the trajectory endpoints. Four trajectory clusters are resolved, and the mean for each cluster are displayed in Fig. 3a. The average source composition associated with each cluster are shown in Fig. 3b.

As shown in Fig. 3, the source compositions exhibit features that agree with the travelled source areas of the corresponding air masses. For example, both fresh and aged sea salt contributions are higher when the monitoring site is under influence by marine air mass (cluster 2 to 4) than under influence by continental air mass from the north (cluster 1). It is also noted that the contribution of aged sea salt is higher in cluster 2 and 3. By examining the individual trajectories in these clusters, it can be

seen that cluster 2 is mostly composed of air masses passing through the coastal areas, whereas cluster 3 consists of a mix of marine air masses from the east and short distance continental air masses from the northeast direction (see Fig. S6 in the Supplement). The higher aged sea salt contribution could possibly be explained by the observation that cluster 2 and 3 have more mixed contributions from sea salt and HNO_3, whereas for the other two clusters either there is a deficiency in the
275 availability of sea salt as in cluster 1 or deficiency in HNO_3 as in cluster 4.

The magnitude of total dust contribution exhibits a descending order from cluster 1 to 4, corresponding to a transition from continental air mass from the north to coastal air mass from northeast/east, and to oceanic air mass from the south (Fig. 3). The results suggest the inner continental region to the north of Hong Kong could be a significant dust emitting area, with source intensity strong enough to influence the dust aerosol burden in Hong Kong through regional transport. Recent studies on
280 anthropogenic air pollutant emissions in Guangdong Province (a larger geographical territory of GBA) based on emission inventory development showed that dust source and industrial process source are the main contributors of PM_{10} loading (Bian et al., 2019; Huang et al., 2021). For those emission inventories, the dust source mainly consists of road dust and construction dust emissions, whereas the industrial process source includes emissions from the manufacturing processes of a list of raw materials, including paper, rubber, steel, ceramics, cement, etc. Analysing the hourly field measurement data for elemental
285 species with PMF approach, Zhou et al. (2018) resolved two dust-related source categories responsible for the atmospheric PM_{coarse} loading in Foshan city of Guangdong Province. The first category is road dust with brake and tire wear, while the second is construction dust. Being one of the most important industrial hubs in the GBA, the Foshan city could represent one of source areas responsible for the degraded air quality in Hong Kong imposed by regional transport of air pollutants.

The source nature of our dust factors is inferred by comparing our factor profiles with those in Zhou et al (2018). We noted
290 the chemical profile of their PMF factor containing road dust is similar to that of our third factor, both accounting for over half of the coarse Al, Si, K, Ca, Ti and Fe by mass, inferring contributions from road dust. The elemental ratios of our third factor are also close to that of the local paved road dust reported by Ho et al. (2003); for example, 0.39 in our study vs. 0.39 in Ho et al.'s work for Al/Si, 0.30 vs. 0.46 for Ca/Si, and 0.23 vs. 0.26 for Fe/Si. Aside from road dust, industrial emissions and coal combustion could also be the contributors due to the presence of Zn and Pb. High loadings of both Zn and Pb is also seen in
295 the industrial coal combustion factor by Zhou et al. (2018). Tire wear could also be a potential source of Zn (Pant and Harrison, 2013; Zhou et al., 2018). The carbonaceous components in this factor can be attributed to deposition of combustion emissions on aerosol dust and emission of biological aerosols. Taken together, this dust factor is named "soil dust/industrial and coal combustion". The term soil dust is used instead of road dust because soil dust is broader, covering both road dust and desert dust potentially contributed by desert or loose soil dust from the inner continental region to the north of Hong Kong, inferred
300 from Fig. 3 that cluster 1 samples have the highest dust contribution.

Both the construction dust factor of Zhou et al. (2018) and our fourth factor differ from the first dust factor by a higher abundance of Ca than Si, while deplete in Al, Si, and K. The enrichment in Ca can be regarded as an indication of construction activity. This element is enriched in construction dust because of the use of cementitious materials. A point to note is that the

fourth factor contains a high loading of Cu. Common sources of Cu in PM$_{coarse}$ include brake wear generated from abrasion of

305   brake lining material and brake discs (Pant and Harrison, 2013) and industrial emissions (Taiwo et al., 2014). However, no

coarse mode Cu was reported in the PMF factor profiles by Zhou et al., and hence it remains uncertain to what extent the fourth

factor resolved in this study is similar to the construction dust factor resolved by Zhou et al. Considering the additional presence

of the characteristic Cu peak, the fourth factor is termed "construction dust/copper-rich emissions".
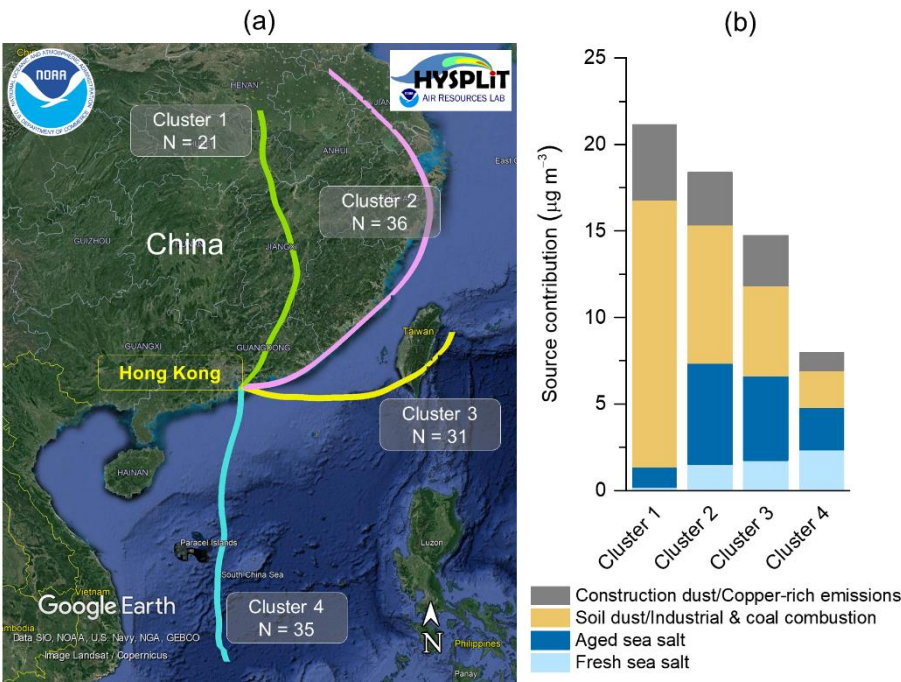
310   **Figure 3. Source contributions to PM$_{coarse}$ grouped by air masses associated with different back-trajectory clusters. Past 48-hour**
backward trajectory of air mass reaching Hong Kong (height = 300 m above ground level) during the end of each sampling event at
midnight are considered. Figure (a) shows the mean trajectories of the four clustered trajectories (Map data: Google Earth, Data
SIO, NOAA, U.S. Navy, NGA, GEBCO, Image Landsat/Copernicus) while Fig. (b) shows the source contributions for the
corresponding clusters.

315   **3.3 Characterization of the unidentified PM$_{coarse}$ mass**

As mentioned in Sect. 2.3, the total PM$_{coarse}$ mass was considered in PMF modeling as a total variable. The apportioned masses

show an excellent agreement with measurements, with R^2 value of 0.98 and slope of 1.04 (intercept = –0.57). A test was

performed to examine if including the total mass would affect the source apportioning. It shows that inclusion of total mass

has a negligible impact on the PMF solution. Specifically, the apportioning of all individual species is unaffected after

320   including PM$_{coarse}$ mass as a total variable (see Table S1 in the Supplement). The test result implies that the PM$_{coarse}$ mass in

its entirety can be explained by the resolved sources. Based on this finding, the unidentified mass can be allocated to the

individual sources by taking the difference between the PMF-apportioned mass and reconstructed mass in individual factors.

The unidentified mass derived from PMF (average = 5.2 μg m^{-3}) shows reasonable agreement with that from direct subtraction using speciation data (average = 4.1 μg m^{-3}), with R^2 of 0.70 and slope of 1.07. The soil dust/industrial and coal combustion factor represents the largest contributor to the unidentified mass, contributing 46 % (2.4 μg m^{-3}). The contribution by construction dust/Cu-rich emissions is 23 % (1.2 μg m^{-3}). Carbonate, a potentially important component in PM$_{coarse}$, is typically enriched with dust particles. As carbonate was not measured in this study, its quantity is estimated by two methods. The first method assumes all the excess cationic charge is balanced by carbonate. This method gives an average contribution of 0.6 μg m^{-3}. The second method assumes all Ca detected is in the form of CaCO$_3$. The resulting carbonate contribution is 1.5 μg m^{-3} and is construed as the upper estimate. Considering Ca is mostly (98%) apportioned to the two dust factors, carbonate at most accounts for 42 % of the unidentified mass in the combined dust factors (3.6 μg m^{-3}), thus suggesting other unmeasured constituents exist.

It is reported that residue liquid water content (LWC) could be an important contributor to the unidentified mass in PM samples even at low relative humidity (RH) condition for gravimetric measurement (Hueglin et al., 2005). The thermodynamic equilibrium model ISORROPIA II (http://nenes.eas.gatech.edu/ISORROPIA) is applied to estimate the aerosol LWC under the RH and temperature conditions of gravimetric measurement in the balance laboratory (i.e., temperature = 22 ^{o}C, RH = 35 %) (Fountoukis and Nenes, 2007). The calculation is performed assuming an open system in which only aerosol phase concentrations are considered, and the aerosol is in metastable state. When comparing the LWC with individual soluble ions, including Na$^+$, Mg^{2+}, K$^+$, Ca^{2+}, Cl$^-$, nitrate and sulfate (shown in Fig. S5 in the Supplement), we find moderate to strong correlations between LWC and ions associated with sea salt: Na$^+$, Mg^{2+}, Cl$^-$, and nitrate (R^2 = 0.49–0.78). By contrast, sulfate, Ca^{2+}, and K$^+$ appear to be less relevant ($R^2 < 0.15$). The results imply that sea salt components play a key role in governing the LWC in PM$_{coarse}$. The average LWC is estimated to be 1.2 μg m^{-3}, which agrees with the unidentified mass (1.6 μg m^{-3}) in the combined fresh and aged sea salt factors. The unidentified mass in aged sea salt mixed with secondary inorganic aerosols being higher than fresh sea salt (1.3 vs. 0.3 μg m^{-3}) is in line with the fact that NaNO$_3$ is more hygroscopic than NaCl.

After including carbonate and residue LWC, about half of the PMF-apportioned PM mass remains unidentified, and this fraction is mainly contributed by the two dust-related factors. The mass discrepancy is likely attributed to the underprediction of geological mass in the mass reconstruction method, which only accounts for oxides of crustal elements. It is documented that other mineral constituents can exist in soil dust. For example, a field study in Morocco showed that over half of the PM$_{coarse}$ mass was made up of silicates (Kandler et al., 2009). Silicates commonly exist as illite and chloritoid, which contain mineral-bound water that is not considered in thermodynamic equilibrium model. Determining the missing components in the aerosol dust and achieving a mass closure require further investigation with different techniques (e.g., microscopy). Overall, the results from the analysis of unidentified mass are consistent with the established knowledge. It provides support to the source apportionment results for the observed coarse particulates in its entirety, forming a strong basis for understanding their source contributions.

3.4 Source contributions to PM$_{coarse}$

3.4.1 Seasonal variation

Figure 4 presents the absolute and relative source contributions by season in ascending order of PM$_{coarse}$ concentration. The secondary nitrate represents the nitrate from all factors to better characterize the contribution by nitrogen oxides (NO$_x$) emission. The two nitrate-free sea salt factors are aggregated into one sea salt factor. During summer when oceanic wind from the south prevails and ambient PM$_{coarse}$ is the lowest in concentration, sea salt contributes nearly half of the PM$_{coarse}$, representing the most important contributor in this season (47 % or 3.7 μg m^{-3}). Note that the source contributions are based on the PMF-apportioned mass, thus the contributions include residue LWC, which is mainly associated with enhanced uptake of water by aged sea salt aerosols. The soil dust/industrial and coal combustion factor accounts for 24 % (1.8 μg m^{-3}) of the PM$_{coarse}$, followed by secondary nitrate (16 % or 1.2 μg m^{-3}) and the construction dust/Cu-rich emissions factor (13 % or 1.0 μg m^{-3}). The source composition changes slightly in the first winter and spring periods when PM$_{coarse}$ is higher, with sea salt and soil dust/industrial and coal combustion similarly contributing to one third of the PM$_{coarse}$ in both periods. The rest is evenly shared by the other two sources in both periods, i.e., 18–19 % for secondary nitrate and 14–17 % for construction dust/ Cu-rich emissions.

The significantly elevated PM$_{coarse}$ concentration observed in fall and the second winter is driven by the increase in dust contribution, which can be attributed to the prevailing northerlies from continental region. The two dust-related factors impose a disproportionate impact on the ambient PM$_{coarse}$ loading during these two seasons, contributing three quarters (72–79 %) of the PM$_{coarse}$ mass in total. Compared to summer, the total contribution is 5 times or more higher in fall and the second winter, being 16.0 and 19.8 μg m^{-3}, respectively. The seasonal difference is consistent with an earlier source apportionment study by Yuan et al. (2013), in which an 11 year long (1998–2008) speciation data set obtained from the Hong Kong PM$_{10}$ network was analyzed by receptor modeling approach. Specifically, the study reported a 3 times higher crustal soil/dust contribution to PM$_{10}$ in winter than in summer (9.7 vs. 3.2 μg m^{-3}). Moreover, it showed the contributions of this source category are spatially and temporally similar across different monitoring stations in Hong Kong, implying the regional nature of this source.

The Foshan source apportionment study of Zhou et al. (2018) mentioned earlier was conducted in October–December 2014. Assuming the difference between PM$_{10}$ and PM$_{2.5}$ contributions by their motor vehicles/road dust factor is due to road dust, their road dust and construction dust sources contributed to 17.7 and 9.4 μg m^{-3} of PM$_{coarse}$, respectively. These contributions are higher than the 12.9–15.2 μg m^{-3} and 3.2–4.6 μg m^{-3} levels estimated for the soil dust/industrial and coal combustion and construction dust/Cu-rich emissions factors in fall and second winter of this study. This spatial gradient lends support to that the dust contributions in Hong Kong is associated with regional transport. Once entrained into the atmosphere, the lifetime of mineral dust can be up to several days and therefore it can be transported over long distance (over thousands of kilometers) and the concentration would decrease with transport distance away from the source regions.
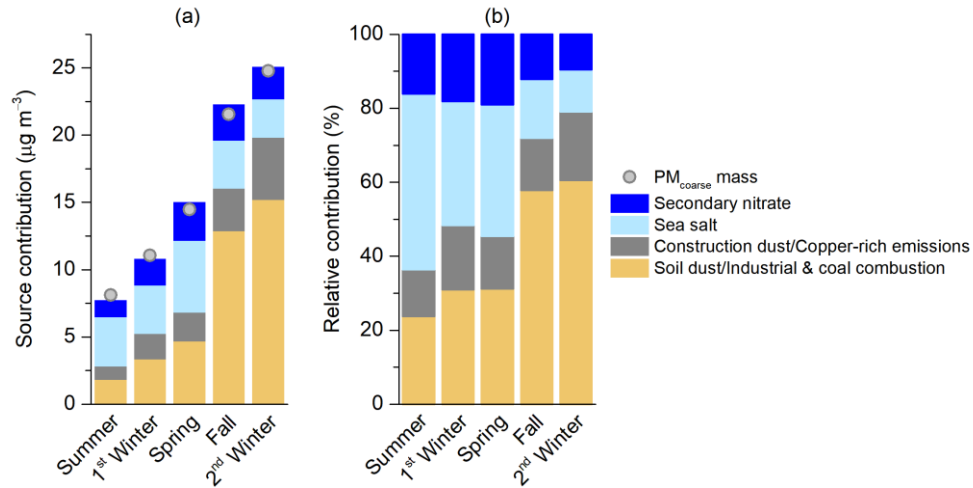
Figure 4. Source contributions to PM$_{coarse}$ during the study period. Figure (a) shows the results in μg m^{-3} while Fig. (b) shows the results in percentage share. The circle markers on the left figure represent the PM$_{coarse}$ concentration measured by gravimetric analysis.

3.4.2 Potential source regions

The potential source areas are mapped by coupling the PMF-derived source contributions at the receptor with the associated backward air mass trajectory. In this analysis, the geographical domain of interest is divided and represented by a grid cell matrix. By coupling the trajectory endpoints in the grid cells with the concentrations at the receptor, each grid cell will receive a value representing the potential source strength in the corresponding area. The Concentration-Weighted Trajectory (CWT) method is applied for the analysis (Hsu et al., 2003). In this method, each grid cell receives a weighted concentration value obtained by averaging the sample concentration that has associated trajectories crossing the corresponding grid cell, weighted by the residence time of air mass in that grid cell. The weighted concentration value (or CWT value) is expressed by Eq. (1):

$$CWT_{ij} = \frac{\sum_{l=1}^{L} C_l \tau_{ijl}}{\sum_{l=1}^{L} \tau_{ijl}} \tag{1}$$

where C_l is the concentration at the receptor site associated with back-trajectory l, τ_{ijl} is the number of endpoints of trajectory l falling into gird cell i,j (i.e., the residence time of the trajectory in the grid cell), and L is the total number of trajectories over a time period. To improve the robustness of the CWT analysis, the input trajectory information was augmented by considering all the trajectories calculated every three hours for each sampling day and assuming the same concentrations over the day (Petit et al., 2017). The geographical domain was defined based on the spatial range of the trajectories traveled, with the dimension of grid cells set to be 0.5° × 0.5°. A weighting function was applied to down-weight grid cells with insufficient number of endpoints following the software guidelines. The CWT analysis was performed using the Zefir program (Petit et al., 2017). The analysis was performed by season to account for the potential variability in source strength and meteorological conditions. Figure 5 presents the CWT results for summer and the second winter and indicates the potential source areas. The results for other seasons are displayed in Fig. S7 in the Supplement. It can be seen that for the two dust-related factors, the elevated

contributions are associated with continental air masses originated from the north, whereas the sea salt-related contributions

410 are associated with marine and coastal air masses. These results are consistent with the general understanding of source origins of these categories of sources. An important finding revealed from this analysis is that the GBA or the greater part of southern China is shown to have significant fugitive dust-related emission sources and that these dust sources are implicated in causing days of high ambient PM$_{coarse}$ loading in Hong Kong.
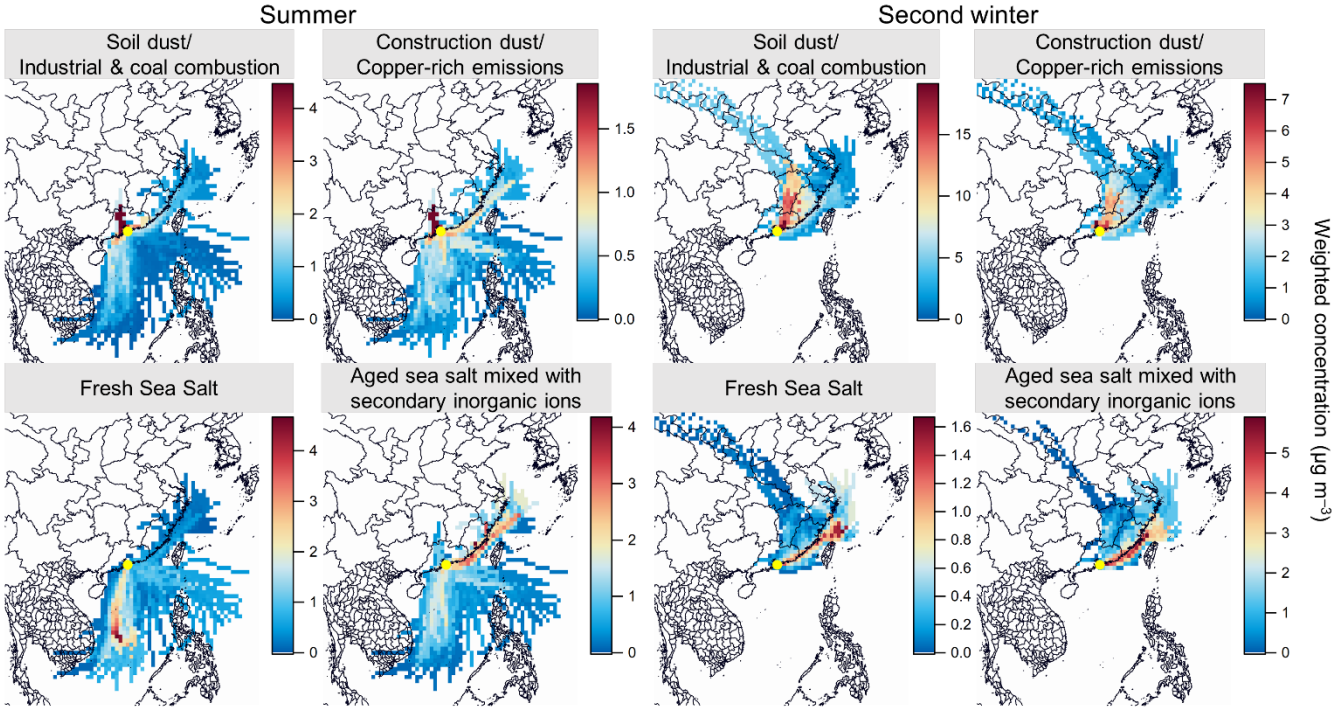
415 **Figure 5. Concentration-Weighted Trajectory results for individual PM$_{coarse}$ contributing sources in summer and the second winter. The location of the receptor site (Hong Kong) is represented by the yellow marker. The results for the other seasons are provided in Fig. S7 in the Supplement.**

3.5 Implications to atmospheric research and public health

As indicated in two field studies measuring size segregated PM composition in Hong Kong, the distribution of nitrate in fine

420 and coarse mode particles in coastal environment depends on the amount of gaseous HNO$_3$ and alkaline particles (e.g., sea salt and soil dust) (Bian et al., 2014; Xue et al., 2014). The former is mainly controlled by the NH$_4$NO$_3$–NH$_3$ + HNO$_3$ equilibrium that is closely related to fine particles pH, temperature, and relative humidity, while the latter was shown to be more closely related to sea salt. The source apportionment analysis for PM$_{coarse}$ in this study reaffirms sea salt plays a dominant role in the uptake of HNO$_3$ in our coastal environment. Based on the PMF results, 77 % of coarse nitrate is associated with sea salt, with

425 the rest associated with fugitive dust. Despite the fact that fugitive dust-related aerosols represent a significant part of PM$_{coarse}$ loading in our study area, this component has a less important role to play in coarse nitrate formation. Nonetheless, the results

indicate that controlling HNO_3 precursors would reduce nitrate in both $PM_{2.5}$ and PM_{coarse}. A limitation to note is that the aerosol samples collected in this study were not corrected for sampling artifact of nitrate, which would affect the accuracy of the measured nitrate concentrations. The extent of the nitrate sampling artifact is expected to be temperature-dependent and

430   aerosol chemical composition-dependent, therefore varies from day-to-day. This variable nature makes its correction difficult. The effect of this type of artifact on coarse nitrate measurement warrants further investigation. The possible inter-particle interaction between fine and coarse particles on the PM_{10} samples is also neglected, which potentially bias the nitrate measurements in the two size modes.

The comprehensive and high quality PM_{coarse} speciation and source apportionment results identify fugitive dust as the

435   significant contributor to PM_{coarse}, especially during high PM_{coarse} days. It should be noted that the high loading of dust was not caused by transient dust storm events, but occurred over the entire fall and winter season, indicating the constant emission of dust particles. A recent study conducted in northern China showed that coarse dust particles can act as a medium for rapid secondary inorganic and organic aerosols formation in highly polluted condition (Xu et al., 2020). Considering the southern China is more humid than northern China, our study region presents an atmospheric condition different from that in Xu et al.'s

440   study, which is more favourable to adsorption of water on mineral dust, and consequently lead to different impacts on atmospheric chemistry and climate (Tang et al., 2016). In this study, 90 % of coarse OC are apportioned to the two dust-related factors by PMF. Given both $PM_{2.5}$ and PM_{coarse} in our study region typically experience long transport distance, more detailed speciation on organic markers might be helpful in elucidating the natural vs. anthropogenic and primary vs. secondary nature of the organics in PM_{coarse}.

445   Accumulative evidence has shown the positive link between adverse health effects and PM_{coarse} exposure. Nationwide studies in China have provided evidence for the association between short-term exposure to PM_{coarse} and mortality and reduced pulmonary function in adult asthmatic patients (Chen et al., 2019; Lei et al., 2022). These studies indicate a stronger association in southern China compared to the northern part, which might be attributed to the difference in the source composition. For example, dust aerosols in the north typically contain higher proportion of windblown dust from natural sources while those in

450   the south might have larger influence from industrial and traffic-related emissions. Oxidative potential of PM has been shown to be a useful metric for PM health impact. Copper and humic-like substances (HULIS) are important active species in catalysing the formation of reactive oxygen species leading to oxidative stress in human body (Lin and Yu, 2011; Bates et al., 2019). The former is likely found in industrial emissions and non-tailpipe emissions (brake/tire wear) while the latter are likely associated with biological material in soil. In this study, the average concentrations of fine and coarse mode Cu are comparable,

455   being 8.1±5.4 and 7.6±4.7 ng m^{-3}, respectively. Given that Cu is the important species governing the response of acellular assay for PM oxidative potential measurement, the similar magnitude in concentration calls for further investigation into the sources and potential health effects of PM_{coarse}.

4 Conclusions

PM$_{coarse}$ has an important role to play in formulating policies to control PM$_{10}$ given its growing relative contribution to PM$_{10}$
460 loading in urban atmospheres. We have conducted the first joint chemical speciation of PM$_{10}$ and PM$_{2.5}$ in Hong Kong, a
coastal and highly urbanized city in southern China. This enables us to derive a high quality PM$_{coarse}$ composition data set
spanning a 1 year long period from January 2020 to February 2021. The annual average concentration of PM$_{coarse}$ is 14.9±8.6
μg m^{-3} (±standard deviation), representing nearly half (45 %) of ambient PM$_{10}$ (32.9±18.5 μg m^{-3}). The PM$_{coarse}$ also exhibit a
large seasonal variation, ranging from 8.1 μg m^{-3} in summer to 24.8 μg m^{-3} in the second winter period. Meteorological data
465 suggest the seasonal contrast is driven by the variations in emission pattern and/or air mass origin.

Among the measured constituents, geological material calculated by assuming oxides of crustal elements represents the largest
PM$_{coarse}$ component (35 %), followed by nitrate (15 %), sea salt ions (11 %) and organics (8 %). A quarter of PM$_{coarse}$ mass
(4.1 μg m^{-3}) was regarded as unidentified mass according to a mass closure analysis. Positive matrix factorization analysis
apportioned the PM$_{coarse}$ mass to four sources, including soil dust/industrial & coal combustion, construction dust/copper-rich
470 emissions, fresh sea salt, and aged sea salt mixed with secondary inorganic aerosols. Additionally, these four sources are able
to account for the unidentified mass. The results show that ~70 % of the unidentified mass is associated with the two dust
factors, while the rest is residue liquid water content as implied from thermodynamic modeling using ISORROPIA II.

The source composition of PM$_{coarse}$ exhibits a distinct seasonal variation, mainly resulting from the changes in the source area
the air mass has travelled. In summer when the site mainly receives air mass travelled from the sea, sea salt components
475 represent the largest contributor (47 %), followed by the two dust-related factors (38 % in total). In fall and winter when the
site is under the influences of air masses travelled from the northern continental region, the two dust-related factors dominate
the ambient PM$_{coarse}$ burden, constituting 72–79 % of the PM$_{coarse}$ mass in total. Additionally, this study shows that the majority
of coarse nitrate (77 %) is formed via reaction with sea salt, with the rest being associated with fugitive dust.

The source contribution and back-trajectory results were coupled and analyzed by the Concentration-Weighted Trajectory
480 method to map the potential source areas. The results show that either the Greater Bay Area or the greater part of southern
China have a source intensity of fugitive dust-related emissions sufficiently large to result in the high ambient PM$_{coarse}$ loadings
in Hong Kong, especially when the meteorological condition is favourable to regional transport of air pollutants. This study
identified several aspects for further PM$_{coarse}$ or PM$_{10}$ research, including pinpointing the exact dust generation processes
leading to the high PM$_{coarse}$ loadings in the study region, elucidating the roles of coarse particles in mediating secondary aerosol
485 formation, and examining the potential health burden of PM$_{coarse}$ exposure through oxidative potential measurement.

Data availability. Chemical composition data presented in this study can be requested by emailing enquiry@epd.gov.hk or contacting the corresponding authors (envrykwong@ust.hk; jian.yu@ust.hk).

Author contribution. YKW, JZY and KKML formulated the overall design of the study. YKW, KML, and CY carried out the chemical analyses. YKW analyzed the data with contributions from JZY and KKML. YKW and JZY prepared the manuscript with contributions from all co-authors.

Competing interests. The authors declare that they have no conflict of interest.

Disclaimer. The content of this paper does not necessarily reflect the views and policies of the HKSAR Government, nor does mention of trade names or commercial products constitute an endorsement or recommendation of their use.

Acknowledgements. This work is supported by the Hong Kong Environmental Protection Department (HKEPD) (tender refs. 19-01121 and 19-01177). We thank Robert Tang and Rebecca Kwan of HKEPD for their inputs and assistance in project logistics. We gratefully acknowledge the NOAA Air Resources Laboratory (ARL) for the provision of the HYSPLIT transport and dispersion model used in this publication.

References

Adar, S. D., Filigrana, P. A., Clements, N., and Peel, J. L.: Ambient coarse particulate matter and human health: A systematic review and meta-analysis, Curr. Environ. Health Rep., 1, 258–274, https://doi.org/10.1007/s40572-014-0022-z, 2014.

Bates, J. T., Fang, T., Verma, V., Zeng, L. H., Weber, R. J., Tolbert, P. E., Abrams, J. Y., Sarnat, S. E., Klein, M., Mulholland, J. A., and Russell, A. G.: Review of acellular assays of ambient particulate matter oxidative potential: Methods and relationships with composition, sources, and health effects, Environ. Sci. Technol., 53, 4003–4019, https://doi.org/10.1021/acs.est.8b03430, 2019.

Bian, Q. J., Huang, X. H. H., and Yu, J. Z.: One-year observations of size distribution characteristics of major aerosol constituents at a coastal receptor site in Hong Kong – Part 1: Inorganic ions and oxalate, Atmos. Chem. Phys., 14, 9013–9027, https://doi.org/10.5194/acp-14-9013-2014, 2014.

Bian, Y. H., Huang, Z. J., Ou, J. M., Zhong, Z. M., Xu, Y. Q., Zhang, Z. W., Xiao, X., Ye, X., Wu, Y. Q., Yin, X. H., Li, C., Chen, L. F., Shao, M., and Zheng, J. Y.: Evolution of anthropogenic air pollutant emissions in Guangdong Province, China, from 2006 to 2015, Atmos. Chem. Phys., 19, 11701–11719, https://doi.org/10.5194/acp-19-11701-2019, 2019.

Chen, R. J., Yin, P., Meng, X., Wang, L. J., Liu, C., Niu, Y., Liu, Y. N., Liu, J. M., Qi, J. L., You, J. L., Kan, H. D., and Zhou, M. G.: Associations between coarse particulate matter air pollution and cause-specific mortality: A nationwide analysis in 272 Chinese cities, Environ. Health Perspect., 127, 017008, https://doi.org/10.1289/ehp2711, 2019.

Cheng, Y., Lee, S. C., Gu, Z. L., Ho, K. F., Zhang, Y. W., Huang, Y., Chow, J. C., Watson, J. G., Cao, J. J., and Zhang, R. J.:

515     $PM_{2.5}$ and $PM_{10-2.5}$ chemical composition and source apportionment near a Hong Kong roadway, Particuology, 18, 96–104, https://doi.org/10.1016/j.partic.2013.10.003, 2015.

Cheung, K., Daher, N., Kam, W., Shafer, M. M., Ning, Z., Schauer, J. J., and Sioutas, C.: Spatial and temporal variation of chemical composition and mass closure of ambient coarse particulate matter ($PM_{10-2.5}$) in the Los Angeles area, Atmos. Environ., 45, 2651–2662, https://doi.org/10.1016/j.atmosenv.2011.02.066, 2011.

520   Chow, J. C. and Watson, J. G.: Guideline on speciated particulate monitoring, prepared by Desert Research Institute, Reno, NV, for the U. S. Environmental Protection Agency, Research Triangle Park, NC, 1998.

Chow, J. C., Watson, J. G., Chen, L. W. A., Chang, M. C. O., Robinson, N. F., Trimble, D., and Kohl, S.: The IMPROVE_A temperature protocol for thermal/optical carbon analysis: maintaining consistency with a long-term database, J. Air Waste Manage., 57, 1014–1023, https://doi.org/10.3155/1047-3289.57.9.1014, 2007.

525   Clements, A. L., Fraser, M. P., Upadhyay, N., Herckes, P., Sundblom, M., Lantz, J., and Solomon, P. A.: Chemical characterization of coarse particulate matter in the Desert Southwest – Pinal County Arizona, USA, Atmos. Pollut. Res., 5, 52–61, https://doi.org/10.5094/APR.2014.007, 2014.

Cohen, D. D., Garton, D., Stelcer, E., Hawas, O., Wang, T., Poon, S., Kim, J., Choi, B. C., Oh, S. N., Shin, H. J., Ko, M. Y., and Uematsu, M.: Multielemental analysis and characterization of fine aerosols at several key ACE-Asia sites, J. Geophys.

530   Res.-Atmos., 109, D19S12, https://doi.org/10.1029/2003JD003569, 2004.

Daher, N., Ruprecht, A., Invernizzi, G., De Marco, C., Miller-Schulze, J., Heo, J. B., Shafer, M. M., Shelton, B. R., Schauer, J. J., and Sioutas, C.: Characterization, sources and redox activity of fine and coarse particulate matter in Milan, Italy, Atmos. Environ., 49, 130–141, https://doi.org/10.1016/j.atmosenv.2011.12.011, 2012.

Edgerton, E. S., Casuccio, G. S., Saylor, R. D., Lersch, T. L., Hartsell, B. E., Jansen, J. J., and Hansen, D. A.: Measurements

535   of OC and EC in coarse particulate matter in the Southeastern United States, J. Air Waste Manage., 59, 78–90, https://doi.org/10.3155/1047-3289.59.1.78, 2009.

Fountoukis, C. and Nenes, A.: ISORROPIA II: A computationally efficient thermodynamic equilibrium model for K^+–Ca^{2+}–Mg^{2+}–NH_4^+–Na^+–SO_4^{2-}–NO_3^-–Cl^-–H_2O aerosols, Atmos. Chem. Phys., 7, 4639–4659, https://doi.org/10.5194/acp-7-4639-2007, 2007.

540   Hand, J. L., Gill, T. E., and Schichtel, B. A.: Urban and rural coarse aerosol mass across the United States: Spatial and seasonal variability and long-term trends, Atmos. Environ., 218, 117025, https://doi.org/10.1016/j.atmosenv.2019.117025, 2019.

Harrison, R. M., Jones, A. M., and Lawrence, R. G.: Major component composition of PM_{10} and $PM_{2.5}$ from roadside and urban background sites, Atmos. Environ., 38, 4531–4538, https://doi.org/10.1016/j.atmosenv.2004.05.022, 2004.

HKEPD: Air quality in Hong Kong 2019, Hong Kong Environmental Protection Department, Hong Kong,

545   https://www.aqhi.gov.hk/api_history/english/report/files/AQR2019e_final.pdf, 2020.

Ho, K. F., Lee, S. C., Chow, J. C., and Watson, J. G.: Characterization of PM_{10} and $PM_{2.5}$ source profiles for fugitive dust in Hong Kong, Atmos. Environ., 37, 1023–1032, https://doi.org/10.1016/S1352-2310(02)01028-2, 2003.

Hsu, Y. K., Holsen, T. M., and Hopke, P. K.: Comparison of hybrid receptor models to locate PCB sources in Chicago, Atmos. Environ., 37, 545–562, https://doi.org/10.1016/S1352-2310(02)00886-5, 2003.

550 Huang, X. H. H., Bian, Q. J., Ng, W. M., Louie, P. K. K., and Yu, J. Z.: Characterization of $PM_{2.5}$ major components and source investigation in suburban Hong Kong: A one year monitoring study, Aerosol Air Qual. Res., 14, 237–250, https://doi.org/10.4209/aaqr.2013.01.0020, 2014.

Huang, Z. J., Zhong, Z. M., Sha, Q. G., Xu, Y. Q., Zhang, Z. W., Wu, L. L., Wang, Y. Z., Zhang, L. H., Cui, X. Z., Tang, M. S., Shi, B. W., Zheng, C. Z., Li, Z., Hu, M. M., Bi, L. L., Zheng, J. Y., and Yan, M.: An updated model-ready emission
555 inventory for Guangdong Province by incorporating big data and mapping onto multiple chemical mechanisms, Sci. Total Environ., 769, 144535, https://doi.org/10.1016/j.scitotenv.2020.144535, 2021.

Hueglin, C., Gehrig, R., Baltensperger, U., Gysel, M., Monn, C., and Vonmont, H.: Chemical characterisation of $PM_{2.5}$, PM_{10} and coarse particles at urban, near-city and rural sites in Switzerland, Atmos. Environ., 39, 637–651, https://doi.org/10.1016/j.atmosenv.2004.10.027, 2005.

560 Jiang, S. Y. N., Gali, N. K., Yang, F. H., Zhang, J. K., and Ning, Z.: Chemical characterization of size-segregated PM from different public transport modes and implications of source specific contribution to public exposure, Environ. Sci. Pollut. Res., 24, 20029–20040, https://doi.org/10.1007/s11356-017-9661-6, 2017.

Kandler, K., Schütz, L., Deutscher, C., Ebert, M., Hofmann, H., Jäckel, S., Jaenicke, R., Knippertz, P., Lieke, K., Massling, A., Petzold, A., Schladitz, A., Weinzierl, B., Wiedensohler, A., Zorn, S., and Weinbruch, S.: Size distribution, mass
565 concentration, chemical and mineralogical composition and derived optical parameters of the boundary layer aerosol at Tinfou, Morocco, during SAMUM 2006, Tellus B, 61, 32–50, https://doi.org/10.1111/j.1600-0889.2008.00385.x, 2009.

Lei, J., Yang, T., Huang, S. J., Li, H. C., Zhu, Y. X., Gao, Y., Jiang, Y. X., Wang, W. D., Liu, C., Kan, H. D., and Chen, R. J.: Hourly concentrations of fine and coarse particulate matter and dynamic pulmonary function measurements among 4992 adult asthmatic patients in 25 Chinese cities, Environ. Int., 158, 106942, https://doi.org/10.1016/j.envint.2021.106942, 2022.

570 Lin, P. and Yu, J. Z.: Generation of reactive oxygen species mediated by humic-like substances in atmospheric aerosols, Environ. Sci. Technol., 45, 10362–10368, https://doi.org/10.1021/es2028229, 2011.

Louie, P. K. K., Watson, J. G., Chow, J. C., Chen, A., Sin, D. W., and Lau, A. K.: Seasonal characteristics and regional transport of $PM_{2.5}$ in Hong Kong, Atmos. Environ., 39, 1695–1710, https://doi.org/10.1016/j.atmosenv.2004.11.017, 2005.

Norris, G., Duvall, R., Brown, S., and Bai, S.: EPA Positive Matrix Factorization (PMF) 5.0 fundamentals and user guide,
575 prepared for the U. S. Environmental Protection Agency, Office of Research and Development, Washington, DC, https://www.epa.gov/sites/default/files/2015-02/documents/pmf_5.0_user_guide.pdf, 2014.

Paatero, P. and Tapper, U.: Positive matrix factorization: A non-negative factor model with optimal utilization of error estimates of data values, Environmetrics, 5, 111–126. https://doi.org/10.1002/env.3170050203, 1994.

Pant, P. and Harrison, R. M.: Estimation of the contribution of road traffic emissions to particulate matter concentrations from field measurements: A review, Atmos. Environ., 77, 78–97, https://doi.org/10.1016/j.atmosenv.2013.04.028, 2013.

Petit, J. E., Favez, O., Albinet, A., and Canonaco, F.: A user-friendly tool for comprehensive evaluation of the geographical origins of atmospheric pollution: Wind and trajectory analyses, Environ. Model. Softw., 88, 183–187, https://doi.org/10.1016/j.envsoft.2016.11.022, 2017.

Putaud, J. P., Van Dingenen, R., Alastuey, A., Bauer, H., Birmili, W., Cyrys, J., Flentje, H., Fuzzi, S., Gehrig, R., Hansson, H. C., Harrison, R. M., Herrmann, H., Hitzenberger, R., Hüglin, C., Jones, A. M., Kasper-Giebl, A., Kiss, G., Kousa, A., Kuhlbusch, T. A. J., Löschau, G., Maenhaut, W., Molnar, A., Moreno, T., Pekkanen, J., Perrino, C., Pitz, M., Puxbaum, H., Querol, X., Rodriguez, S., Salma, I., Schwarz, J., Smolik, J., Schneider, J., Spindler, G., Brink, H. T., Tursic, J., Viana,M., Wiedensohler, A., and Raes, F.: A European aerosol phenomenology – 3: Physical and chemical characteristics of particulate matter from 60 rural, urban, and kerbside sites across Europe, Atmos. Environ., 44, 1308–1320, https://doi.org/10.1016/j.atmosenv.2009.12.011, 2010.

Stein, A. F., Draxler, R. R., Rolph, G. D., Stunder, B. J., Cohen, M. D., and Ngan, F.: NOAA's HYSPLIT atmospheric transport and dispersion modeling system, Bull. Am. Meteorol. Soc., 96, 2059–2077, https://doi.org/10.1175/BAMS-D-14-00110.1, 2015.

Stone, E., Schauer, J., Quraishi, T. A., and Mahmood, A.: Chemical characterization and source apportionment of fine and coarse particulate matter in Lahore, Pakistan, Atmos. Environ., 44, 1062–1070, https://doi.org/10.1016/j.atmosenv.2009.12.015, 2010.

Taiwo, A. M., Harrison, R. M., and Shi, Z. B.: A review of receptor modelling of industrially emitted particulate matter, Atmos. Environ., 97, 109–120, http://dx.doi.org/10.1016/j.atmosenv.2014.07.051, 2014.

Tang, M., Cziczo, D. J., and Grassian, V. H.: Interactions of water with mineral dust aerosol: water adsorption, hygroscopicity, cloud condensation, and ice nucleation, Chem. Rev., 116, 4205–4259, https://doi.org/10.1021/acs.chemrev.5b00529, 2016.

USEPA: Integrated Science Assessment for Particulate Matter, the U.S. Environmental Protection Agency, Research Triangle Park, NC, https://www.epa.gov/isa/integrated-science-assessment-isa-particulate-matter, 2019.

Turpin, B. J. and Lim, H. J.: Species contributions to $PM_{2.5}$ mass concentrations: Revisiting common assumptions for estimating organic mass, Aerosol Sci. Technol., 35, 602–610, https://doi.org/10.1080/02786820119445, 2001.

Wu, C. and Yu, J. Z.: Evaluation of linear regression techniques for atmospheric applications: The importance of appropriate weighting, Atmos. Meas. Tech., 11, 1233–1250, https://doi.org/10.5194/amt-11-1233-2018, 2018.

Xu, W. Y., Kuang, Y., Liang, L. L., He, Y., Cheng, H. B., Bian, Y. X., Tao, J. C., Zhang, G., Zhao, P. S., Ma, N., Zhao, H. R., Zhou, G. S., Su, H., Cheng, Y. F., Xu, X. B., Shao, M., and Sun, Y.: Dust-dominated coarse particles as a medium for rapid secondary organic and inorganic aerosol formation in highly polluted air, Environ. Sci. Technol., 54, 15710–15721, https://doi.org/10.1021/acs.est.0c07243, 2020.

Xue, J., Yuan, Z. B., Lau, A. K. H., and Yu, J. Z.: Insights into factors affecting nitrate in $PM_{2.5}$ in a polluted high NO_x environment through hourly observations and size distribution measurements, J. Geophys. Res.-Atmos., 119, 4888–4902, http://dx.doi.org/10.1002/2013JD021108, 2014.

Yu, J. Z. and Zhang, T.: Chemical speciation of $PM_{2.5}$ filter samples – January 1 through December 31, 2017, Final report
615 submitted to the Hong Kong Environmental Protection Department, The Government of the Hong Kong Special Administrative Region, 2018.

Yu, J. Z., Tung, J. W. T., Wu, A. W. M., Lau, A. K. H., Louie, P. K. K., and Fung, J. C. H.: Abundance and seasonal characteristics of elemental and organic carbon in Hong Kong PM_{10}, Atmos. Environ., 38, 1511–1521, https://doi.org/10.1016/j.atmosenv.2003.11.035, 2004.

620 Yuan, Z. B., Yadav, V., Turner, J. R., Louie, P. K. K., and Lau, A. K. H.: Long-term trends of ambient particulate matter emission source contributions and the accountability of control strategies in Hong Kong over 1998–2008, Atmos. Environ., 76, 21–31, http://dx.doi.org/10.1016/j.atmosenv.2012.09.026, 2013.

Zhang, X. X., Yuan, Z. B., Li, W. S., Lau, A. K. H., Yu, J. Z., Fung, J. C. H., Zheng, J. Y., and Yu, A. L. C.: Eighteen-year trends of local and non-local impacts to ambient PM_{10} in Hong Kong based on chemical speciation and source apportionment,
625 Atmos. Res., 214, 1–9, https://doi.org/10.1016/j.atmosres.2018.07.004, 2018.

Zhou, S. Z., Davy, P. K., Huang, M. J., Duan, J. B., Wang, X. M., Fan, Q., Chang, M., Liu, Y. M., Chen, W. H., Xie, S. J., Ancelet, T., and Trompetter, W. J.: High-resolution sampling and analysis of ambient particulate matter in the Pearl River Delta region of southern China: Source apportionment and health risk implications, Atmos. Chem. Phys., 18, 2049–2064, https://doi.org/10.5194/acp-18-2049-2018, 2018.